Title	Comparison of different control strategies for energy storage devices
Authors(s)	Ortega, Alvaro; Milano, Federico
Publication date	2016-08-11
Publication information	2016 Power Systems Computation Conference (PSCC)
Conference details	The 19th Power Systems Computation Conference (PSCC 2016), Genova, Italy, 20-24 June 2016
Publisher	IEEE
Link to online version	http://www.pscc2016.net/
Item record/more information	http://hdl.handle.net/10197/10015
Publisher's statement	© 2016 IEEE. Personal use of this material is permitted. Permission from IEEE must be obtained for all other uses, in any current or future media, including reprinting/republishing this material for advertising or promotional purposes, creating new collective works, for resale or redistribution to servers or lists, or reuse of any copyrighted component of this work in other works.
Publisher's version (DOI)	10.1109/PSCC.2016.7540849

Comparison of Different Control Strategies for Energy Storage Devices

Álvaro Ortega
School of Electrical and Electronic Engineering
University College Dublin
Dublin, Ireland
alvaro.ortega-manjavacas@ucdconnect.ie

Federico Milano
School of Electrical and Electronic Engineering
University College Dublin
Dublin, Ireland
federico.milano@ucd.ie

Abstract—This paper compares three control strategies for energy storage devices. Detailed formulations and implementation procedures of PI, sliding mode, and H-infinity controllers are presented and discussed. The dynamic performance of each control technique is also studied and compared. With this aim, the paper duly discusses a comprehensive case study based on the IEEE 14-bus test system with inclusion of a wind power plant and an energy storage device.

Index Terms—Energy Storage System (ESS), H-infinity Control (H_∞), PI Control, Sliding Mode Control (SMC).

I. INTRODUCTION

A. Motivation

The control strategy that has been most widely applied to Energy Storage Systems (ESSs) is the PI, due mainly to its simplicity and easy implementation. It has been shown, however, that the performance of PI controllers can be affected by changes in system operating point and/or topology. For these reasons, alternative robust control strategies have been proposed in the literature for transient stability analysis of ESSs. Among these, we cite Sliding Mode Control (SMC), H-infinity Control (H_∞), Model Predictive Control, and Fuzzy Logic Control. Despite all the variety of control strategies for ESSs, still no comprehensive comparison among such strategies has been provided yet. This paper discusses the mathematical formulation and implementation as well as compares the performance of PI, SMC and H_∞ control strategies. The aim is to provide a fair testbed to determine the features of each controller in terms of robustness against disturbances, e.g., line outages and loss of loads, and uncertainties, e.g., wind power generation.

B. Literature Review

Several works that analyze the behavior of ESSs considering different control strategies for both short term (e.g. transient stability) and long term (e.g. planning) time scales can be found

in the literature. Improved ESSs controllers based on PIs to simultaneously regulate the active and reactive power for Superconducting Magnetic Energy Storage (SMES) and Flywheel Energy Storage (FES) applications are presented in [1] and [2], respectively. In [3], a SMC strategy for a bidirectional DC/DC converter to control the power of an Electrochemical Capacitor Energy Storage (ECES) application is presented, whereas [4] proposes a SMC technique to control a double-fed induction machine used as a FES. A comparison of PI based two-loop control and a SMC of a hybrid ESS is provided in [5]. Finally, robust H_∞ based controls for ESSs are presented in [6] and [7]. The interested reader can find examples of ESSs regulated by Model Predictive and Fuzzy Logic controllers in [8], [9] and [10], respectively.

The models of the devices as well as the controllers presented in this work have been carefully selected from the literature to study the behavior of ESSs considering both voltage and angle stability analysis. Unfortunately, there is still no agreement on a general purpose – yet detailed – model for energy storage devices. The variety of available models is one of the reason for a lack of systematic comparison of different control strategies. In this paper, all controllers are designed using a generalized energy storage device model that we have proposed in [11] and that is briefly outlined in Section II for completeness. This is a fundamental frequency model with inclusion of relevant dynamics on the dc side of the Voltage Source Converter (VSC). The proposed model is taylored for the time scales considered in this work. More detailed models of the VSC connected to the ESS, as well as of its controllers could be considered, e.g., the EMT models proposed in [12]. However, such models are too computationally demanding for the transient stability analysis of interconnected power systems.

C. Contributions

Despite the variety of studies on ESS controllers that can be found in the literature, there is a lack of works that focus on the design and the comparison of different controllers and the identification of the best performing control scheme for ESSs. This paper fills this gap and provides two contributions, as follows:

- A detailed description of the setup and general formulation of PI, SMC and H_∞ control strategies. Implementation issues that arise from each technique are also discussed.

- A fair and comprehensive comparison of the dynamic response and features of each considered control strategy. The case study is aimed to determine the robustness of the controllers against uncertainties, as well as their performance against contingencies and large disturbances.

D. Paper Organization

The paper is organized as follows. Section II presents the structure of a VSC-based ESS connected to the grid, and describes a general model of the ESS device. Section III describes the three control strategies for ESSs studied in this work, and discusses their respective advantages and drawbacks. A comprehensive case study based on the IEEE 14-bus system to understand the performance of each control technique is provided in Section IV. Finally, Section V draws conclusions and outlines future work directions.

II. SCHEME AND MODEL OF THE ENERGY STORAGE SYSTEM

Figure 1 shows the scheme of an energy storage device coupled to a grid. The objective of the ESS is to regulate a measured signal, say w, of the system (e.g., the frequency of the center of inertia, or the active power flowing through a transmission line.). The VSC is modelled using the balanced, fundamental frequency model proposed in [13]–[15], which includes dc circuit and phase-locked loop (PLL) dynamics as well as an average quasi-static phasor model of the converter and an equivalent model for switching losses. The interested reader can find detailed transient stability models of the elements and controllers that regulate the dynamic response of the ESS in [11].
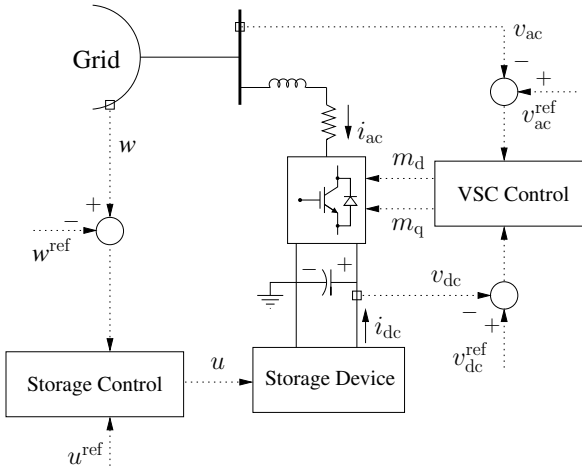

Figure 1: Scheme of an ESS coupled to a grid.

Model of the Energy Storage Device

A generalized model of energy storage devices is used to simulate the dynamic performance of the ESS. This model is based on the observation that most ESSs include potential and flow variables (see Table I), and are connected to the grid through a VSC device. The storage devices are thus modeled as a dipole connected to the dc side of the VSC of Fig. 1. The main advantages of this model are its linear structure

TABLE I: Examples of energy storage technologies.

Types of Storable Energy	Potential Var.	Flow Var.	Device
Magnetic	Magneto Motive Force	Flux	SMES
Fluid	Pressure	Mass Flow	CAES
Electrostatic	Electric Potential	Electric Current	ECES
Electrochemical	Electrochemical Potential	Molar Flow Rate	BES
Rotational	Angular Velocity	Torque	FES

and fixed number of Differential Algebraic Equations (DAEs) for all storage technologies. Both features highly simplify the formulation and implementation of the control strategies that are discussed in this paper. Despite these simplifications, the model considered in this paper appears to be accurate and approximate detailed models well more than other overly simplified ESS models that can be found in the literature. A comprehensive discussion on the accuracy of this generalized ESS model (GEM) is discussed in [11].

The linear time-invariant expression of a generic storage device is given by:

$$\begin{aligned}
\mathbf{\Gamma}_x \dot{\boldsymbol{x}} &= \mathbf{A}_{xx}\boldsymbol{x} + \mathbf{A}_{xz}\boldsymbol{z} + \mathbf{B}_{xu}u + \mathbf{B}_{xv}v_{\mathrm{dc}} + \mathbf{K}_x \\
\mathbf{\Gamma}_z \dot{\boldsymbol{z}} &= \mathbf{A}_{zx}\boldsymbol{x} + \mathbf{A}_{zz}\boldsymbol{z} + \mathbf{B}_{zu}u + \mathbf{B}_{zv}v_{\mathrm{dc}} + \mathbf{K}_z \\
i_{\mathrm{dc}} &= \mathbf{C}_x\boldsymbol{x} + \mathbf{C}_z\boldsymbol{z} + \mathrm{D}_u u + \mathrm{D}_v v_{\mathrm{dc}} + \mathrm{K}_i
\end{aligned} \quad (1)$$

where the state vector $\boldsymbol{x}$ are the potential and flow variables related to the energy stored in the ESS shown in Table I, while $\boldsymbol{z}$ stands for all other variables; u is the output signal of the storage control; v_{dc} and i_{dc} are the dc voltage and current of the VSC, respectively; and $\mathbf{\Gamma} = \mathrm{diag}[\mathbf{\Gamma}_x\ \mathbf{\Gamma}_z]$ is a diagonal matrix such that [16]:

$\Gamma_{ii} = 1$ if the i-th equation of $[\boldsymbol{x}^T\ \boldsymbol{z}^T]^T$ is differential;
$\Gamma_{ii} = 0$ if the i-th equation of $[\boldsymbol{x}^T\ \boldsymbol{z}^T]^T$ is algebraic.

Note that u, v_{dc} and i_{dc} are scalar, whereas all other quantities are vectors. Equation (1) is written for $\boldsymbol{x}$, $\boldsymbol{z}$, u, v_{dc} and i_{dc}, not the incremental values $\Delta\boldsymbol{x}$, $\Delta\boldsymbol{z}$, Δu, Δv_{dc} and Δi_{dc}. With this aim, $\mathbf{K}_x$, $\mathbf{K}_z$ and K_i account for the values of the variables at the equilibrium point.

The dynamic order of (1) is reduced, assuming that the transient response of the variables in $\boldsymbol{z}$ are much faster than those of $\boldsymbol{x}$ (i.e., $\mathbf{\Gamma}_z = \mathbf{0}$). Note that non-singularity of matrix $\mathbf{A}_{zz}$ is required. Therefore, after computing the Schur components of $\boldsymbol{z}$, and rewriting the matrices in compact form, the following set of three DAEs is obtained:

$$\begin{aligned}
\tilde{\mathbf{\Gamma}}\dot{\boldsymbol{x}} &= \tilde{\mathbf{A}}\boldsymbol{x} + \tilde{\mathbf{B}}_u u + \tilde{\mathbf{B}}_v v_{\mathrm{dc}} + \tilde{\mathbf{K}}_x \\
i_{\mathrm{dc}} &= \tilde{\mathbf{C}}\boldsymbol{x} + \tilde{\mathrm{D}}_u u + \tilde{\mathrm{D}}_v v_{\mathrm{dc}} + \tilde{\mathrm{K}}_i
\end{aligned} \quad (2)$$

Finally, the actual value of the energy stored in the device can be computed as follows:

$$E = \sum_{i=1}^{n} \rho_i \left(x_i^{\beta_i} - \chi_i^{\beta_i} \right) \quad (3)$$

where ρ_i, β_i and χ_i are the proportional coefficient, exponential coefficient and reference potential value of each variable x_i, respectively.

The following are relevant remarks on the general model (2), and are also the main conclusion of [11]:

- To obtain the GEM in (2) and (3), the linearization process is applied to the equations of the storage device model, solely. Therefore, energy limits, VSC current limits, and VSC controllers nonlinearity and controlled quantity limits are preserved (see, for example, Fig. 2 and other control schemes provided in [11]). Simulation results provided in [11] allows concluding that such an approximation does not reduce consistently the accuracy of (2) with respect to the fully-fledged nonlinear ESS model.
- To improve the accuracy of the general model above, the matrices in (1) are computed for a median value of the stored energy, i.e., a value equally distant from upper and lower energy limits.

The steps to setup each control strategy considered in this paper are as follows:

1) Main parameters of the ESS are defined through detailed model of the device using data provided from manufacturers.
2) Matrices of the GEM are obtained using the process explained above.
3) The control strategies are implemented based on the GEM, and tested through time domain simulations.
4) Finally, the controller can be directly implemented for the original detailed model of the storage device.

III. ESS Control Strategies

This section describes the three control strategies considered in this paper, namely PI, SMC and H_∞ in subsections III-A, III-B and III-C, respectively. For the SMC and H_∞, the mathematical formulation is also provided. Relevant remarks on practical and numerical implementations of these controllers are also provided in this section.

A. PI Control

A common scheme of a PI-based controller for ESSs is depicted in Fig. 2. This controller takes the deviations of a measured variable of the system, and is typically composed of a dead-band block, a low pass filter, a PI regulator, and a block referred to as Storage Input Limiter, designed to smooth the transients caused by energy saturations of the storage device [17].
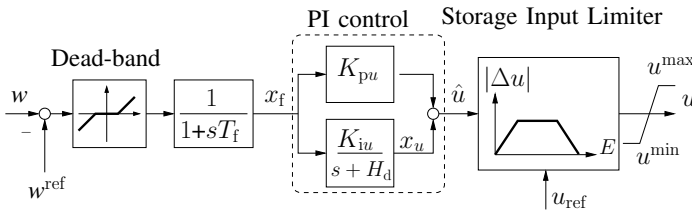

Figure 2: PI-based storage control scheme.

In Fig. 2, the PI controller is composed of a proportional gain, $K_{\mathrm{p}u}$, and an integrator with gain $K_{\mathrm{i}u}$ and integral deviation coefficient H_d. The most common design processes for these gains are trial-and-error and pole-placement techniques. Therefore, the main advantages of this controller are an easy

implementation in power system simulation softwares, and the simplicity in the design process. However, some works show how changes in system topology, as well as operation points that differ from the one for which the PI was designed, may affect the performance of the overall system. In some cases, these changes may lead to instability [5]. This fact has inspired the development of more advanced and robust control techniques aim to substitute or complement the PI regulators. Examples of these alternative controllers are SMC and H_∞ control, which are described in the remainder of this section.

B. Sliding Mode Control

The SMC is a nonlinear control technique that can be applied to *variable structure systems*, i.e., systems that can be modeled as a set of continuous subsystems with a proper switching control logic [18]. Hence, the SMC can be straightforwardly applied to the ESSs that include a DC/DC power converter, such as SCES, SMES, and BES [3], [4]. The switching control logic applied by the SMC, which generally commutes at a high frequency ($\sim$kHz), allows the state of the system to follow a desired trajectory, referred as *sliding surface*, $\mathcal{S}$. If this surface satisfies certain requirements of existence and reachability, the motion associated to the SMC is invariant under bounded uncertainty conditions.

SMC in Linear Systems: The linear structure of the GEM described in Section II highly simplifies the implementation of SMC on ESSs. A linear surface $\mathcal{S}$ for the system described in (2) is considered:

$$\begin{aligned} \mathcal{S} &= s_w x_\mathrm{f} + s_{x_1}(x_1 - x_{10}) + s_{x_2}(x_2 - x_{20}) \\ &= s_w x_\mathrm{f} + \boldsymbol{s}_x(\boldsymbol{x} - \boldsymbol{x_0}) \end{aligned} \quad (4)$$

where x_f is the filtered deviation of the measured signal w to be regulated (see Fig. 2); x_{10} and x_{20} are the values of x_1 and x_2 at the equilibrium point around which the detailed model of the storage device is linearized in order to obtain the GEM in (2), respectively; and s_w and $\boldsymbol{s}_x = [s_{x_1} \ s_{x_2}]$ are control parameters.

The discontinuous output signal of the storage control, u, can be rewritten as the sum of two terms, as follows:

$$u = u_\mathrm{eq} - K_\mathrm{SMC}\,\mathrm{sign}(\mathcal{S}) \quad (5)$$

where u_eq is the continuous component of the control during the sliding mode operation; and K_SMC is a positive gain designed to reduce the effect of external perturbations and disturbances.

If sliding mode operation is reached at a time t_SMC, then $\mathcal{S} = \dot{\mathcal{S}} = 0$ for $t > t_\mathrm{SMC}$. Therefore:

$$\dot{\mathcal{S}} = s_w \dot{x}_\mathrm{f} + \boldsymbol{s}_x \dot{\boldsymbol{x}} = 0 \quad (6)$$

During sliding mode, $\dot{x}_\mathrm{f} = 0$, thus, from (2):

$$\dot{\mathcal{S}} = \boldsymbol{s}_x \tilde{\boldsymbol{\Gamma}}^{-1}\left[\tilde{\mathbf{A}}\boldsymbol{x} + \tilde{\mathbf{B}}_u u + \tilde{\mathbf{B}}_v v_\mathrm{dc} + \tilde{\mathbf{K}}_x\right] = 0 \quad (7)$$

Finally, the continuous component of the control, u_eq, can be computed as follows:

$$u_\mathrm{eq} = -\left(\boldsymbol{s}_x \tilde{\boldsymbol{\Gamma}}^{-1}\tilde{\mathbf{B}}_u\right)^{-1}\boldsymbol{s}_x \tilde{\boldsymbol{\Gamma}}^{-1}\left[\tilde{\mathbf{A}}\boldsymbol{x} + \tilde{\mathbf{B}}_v v_\mathrm{dc} + \tilde{\mathbf{K}}_x\right] \quad (8)$$

Therefore, SMC can be applied to the ESS if $\left(\boldsymbol{s}_x \tilde{\boldsymbol{\Gamma}}^{-1}\tilde{\mathbf{B}}_u\right)^{-1}$ exists.

The robustness against disturbances makes the SMC a promising alternative to PI controllers. However, the main drawbacks of SMC are its involved implementation for non-linear systems, and the so-called *chattering* (i.e., high frequency oscillations derived from deviations from the ideal mathematical model, such as small delays, deadbands and hysteresis).

C. H-infinity Control

Given a linear system, the design of an H_∞ controller consists in finding a feedback matrix that makes the closed-loop system stable and minimizes the influence of external perturbations, disturbances and noises in the output of the system, i.e., minimizes the H_∞ norm of the closed-loop transfer function (see Fig. 3) [6], [7], [19].
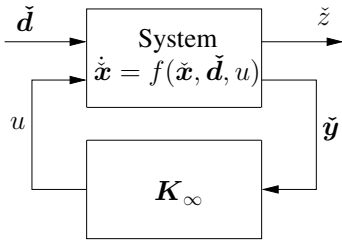
Figure 3: Standard problem of H_∞.

H_∞ *for ESSs:* The reduced order of the GEM in section II, along with its linear structure, allows designing the linear controller K_∞ for ESSs in a systematic way. Using similar notation as in (2), the equations of the upper block in Fig. 3 can be written as follows:

$$\dot{\check{x}} = \check{A}\check{x} + \check{B}_1\check{d} + \check{B}_2 u$$
$$\check{z} = \check{C}_1\check{x} + \check{D}_{11}\check{d} + \check{D}_{12}u \quad (9)$$
$$\check{y} = \check{C}_2\check{x} + \check{D}_{21}\check{d} + \check{D}_{22}u$$

where:

- $\check{x} = [x_1 \ x_2 \ x_u]^T$, where x_1 and x_2 are the state variables of the system in (2); and x_u is the output of the integrator in Fig. 2;
- $\check{d} = [x_f \ v_{dc}]^T$ are the external perturbations;
- $\check{z} = x_u - K_u u$ is the regulated output signal. K_u is a positive weight coefficient to couple the output of the PI controller and the converter of the storage device.
- $\check{y} = [\hat{u} \ v_{dc}]^T$ are the measurement outputs of the system.

Suboptimal solution for K_∞ can be found by solving two algebraic Riccati equations. With this aim, the following assumptions about the system matrices have to be satisfied:

i. $\check{D}_{11} = 0$ and $\check{D}_{22} = 0$;

ii. $\text{rank}\,\check{D}_{12} = \dim u = 1$;

iii. $\text{rank}\,\check{D}_{21} = \dim \check{y} = 2$;

iv. $\text{rank}\begin{bmatrix} j\omega \mathbf{I}_3 - \check{A} & \check{B}_2 \\ \check{C}_1 & \check{D}_{12} \end{bmatrix} = \dim \check{x} + \dim u = 4,$

for all real ω;

v. $\text{rank}\begin{bmatrix} j\omega \mathbf{I}_3 - \check{A} & \check{B}_1 \\ \check{C}_2 & \check{D}_{21} \end{bmatrix} = \dim \check{x} + \dim \check{y} = 5,$

for all real ω.

Once the system in (9) is defined, and all previous assumptions are satisfied, nearly optimal solution for the controller is obtained by solving two Riccati equations of the same order as the system. The Fortran library SLICOT is used to solve these equations [20]. The output provided by this library are the linear matrices of the lower block in Fig. 3, that are used to compute the storage converter input variable, u:

$$\dot{\check{x}}_\infty = \check{A}_\infty \check{x}_\infty + \check{B}_\infty \check{y}$$
$$u = \check{C}_\infty \check{x}_\infty + \check{D}_\infty \check{y} \quad (10)$$

Since the controller is designed in order to minimize the H_∞ norm of the closed-loop transfer function from d to z, the closed-loop system is robust under bounded perturbations and uncertainties in the system. The main issue regarding the H_∞ controllers is that its design is limited to linear or linearized systems exclusively.
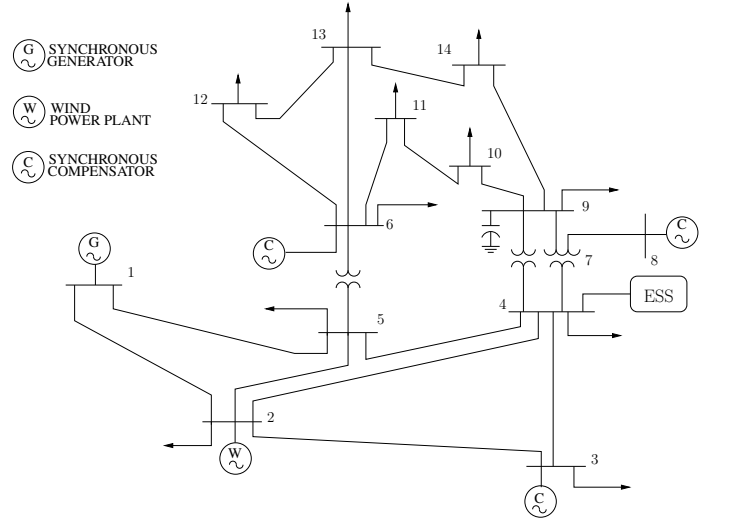
IV. CASE STUDY

Figure 4: IEEE 14-bus test system with an ESS device connected to bus 4.

This section provides a comparison of the dynamic response of the three control strategies discussed above, i.e., PI, SMC and H_∞. With this aim, the IEEE 14-bus test system (see Fig. 4) is used for all simulations. This benchmark network consists of 2 synchronous machines and 3 synchronous compensators, 2 two-winding and 1 three-winding transformers, 15 transmission lines and 11 loads. The system also includes primary voltage regulators (AVRs), turbine governors and an AGC. All dynamic data of the IEEE 14-bus system as well as a detailed discussion of its transient behavior can be found in [21]. Some modifications have been made in this network to study the interaction of the storage device with the rest of the system:

- The capacity of the synchronous generator placed in bus 1 is reduced by 5 times its original value.
- The synchronous generator placed in bus 2 is substituted by a 60-turbines wind power plant of the same power capacity.
- A 30 MW ESS is connected to bus 4.

In this paper, the stochastic process applied to the wind follows a Weibull's distribution [22]:

$$f(v_w, c_w, k_w) = \frac{k_w}{c_w^k} v_w^{k-1} e^{-\left(\frac{v_w}{c_w}\right)^{k_w}} \quad (11)$$

where v_w is the wind speed, and c_w and k_w are the scale and shape factors, respectively. Time variations of the wind speed, $\xi_\mathrm{w}(t)$, are computed as follows:

$$\xi_\mathrm{w}(t) = \left(-\frac{\ln \iota(t)}{c_\mathrm{w}}\right)^{\frac{1}{k_\mathrm{w}}} \qquad (12)$$

where $\iota(t)$ is a uniform variate generator of random numbers ($\iota \in [0, 1]$). Finally, the wind speed is computed setting the initial average speed v_w^a determined at the initialization step as mean speed:

$$\check{v}_\mathrm{w}(t) = (1 + \xi_\mathrm{w}(t) - \xi_\mathrm{w}^\mathrm{a})v_\mathrm{w}^\mathrm{a} \qquad (13)$$

where $\xi_\mathrm{w}^\mathrm{a}$ is the average value of $\xi_\mathrm{w}(t)$. To emulate the auto-correlation of the wind speed, i.e., to avoid unrealistic sudden jumps, the wind speed is processed through a low pass filter before entering into the wind turbine equations.

Values of the mean wind speed, scale and shape factors are taken from [23]. Two wind profiles (low and high mean wind speed) have been used in the simulations, and data have been collected from the months of December and August at the height of 65 meters, respectively.

Two scenarios have been considered to study the performance of the ESS applying the three control strategies: in Subsection IV-A the system faces a line outage, whereas a loss of load is considered in Subsection IV-B.

A. Line Outage

In this subsection, the contingency is the outage of the line that connects buses 2 and 4 at $t = 25$ s, during low wind (Fig. 5) and high wind (Fig. 6) periods. The wind speeds corresponding to this profiles are shown in Figs. 5(a) and 6(a), respectively. The system variable regulated by the ESS is the frequency of the center of inertia (ω_COI), and its evolution is depicted in Figs. 5(b), 5(c) and Figs 6(b), 6(c) for the system without storage device and with storage regulated using each one of the control strategies in Section III. For each controller, same control parameters are used in both scenarios in order to check how different operating conditions can affect their performance. The three controllers are able to greatly reduce the frequency fluctuations of the system before and after the line outage and for the two wind profiles. In both cases, the H_∞ control appears to smooth these fluctuations slightly better than the other techniques.

Finally, Figs. 5(d) and 6(d) show the active power consumed/provided by the ESS. Positive power indicates that the ESS is storing energy, and vice versa. Before the line outage, the three techniques have a similar behavior. After the occurrence of the contingency, however, high frequency oscillations can be appreciated for the SMC, due to the effect of the chattering commented in Subsection III-B.

It is relevant to note that the wind speed variation, and therefore, the change of the initial operating point, does not affect the good performance of any of the controllers.

B. Loss of Load

To study the performance of the ESS regulated by the three controllers facing a large disturbance, the loss of load connected to bus 9 is simulated in this subsection (Fig. 7). The contingency
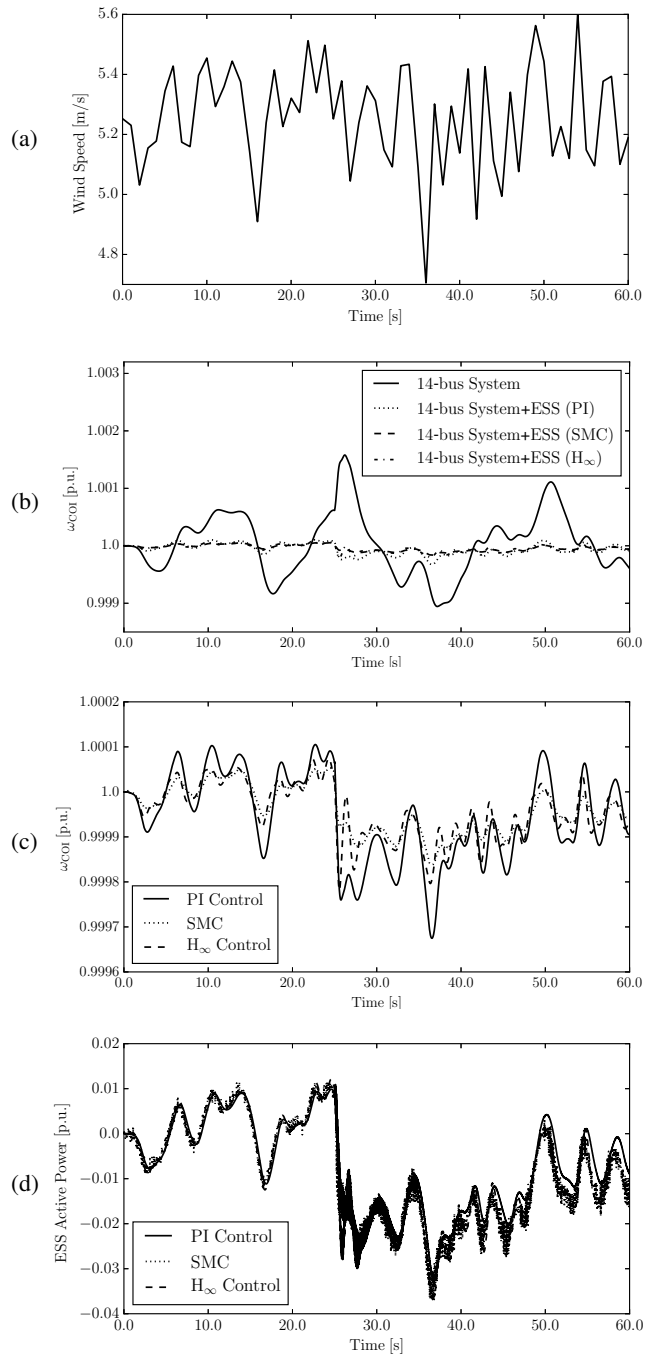

Figure 5: Response of the 14-bus system with an ESS following the opening of line 2-4 for a low wind profile. (a) Wind speed. (b), (c) Frequency of the COI. (d) Active Power of the ESS.

occurs at $t = 25$ s during a high wind period (Fig. 7(a)). The regulated variable is again the ω_COI, and its evolution is shown in Figs. 7(b) and 7(c). The loss of the load causes a peak in the frequency greater than 1.5% (~ 1 Hz) that is not acceptable for the system. The inclusion of the ESS reduces this peak to about 0.6% in the case of the SMC, and about 0.3% in the case of PI and H_∞ controllers. As in the previous cases, the H_∞ control behaves slightly better than the others during the transient, but the performance of the three is fairly similar before and after this transient. As in the previous example, the response
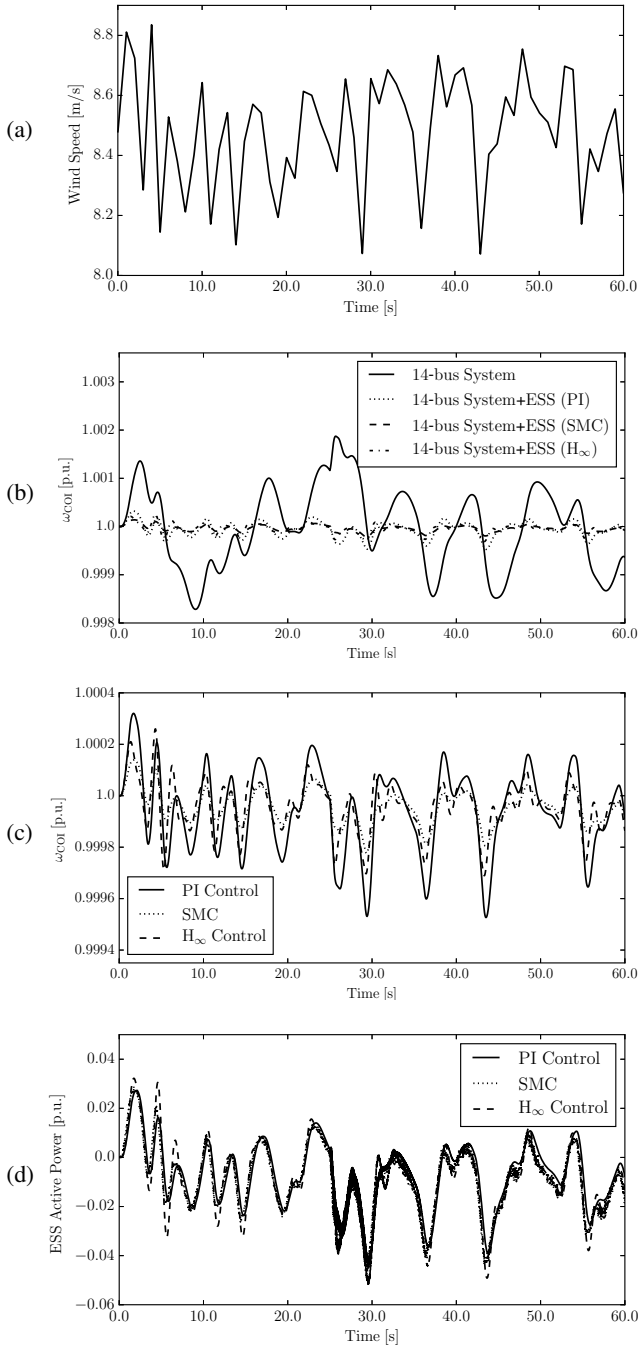
Figure 6: Response of the 14-bus system with an ESS following the opening of line 2-4 for a high wind profile. (a) Wind speed. (b, c) Frequency of the COI. (d) Active Power of the ESS.

Figure 7: Response of the 14-bus system with an ESS following the loss of the load at bus 9 for a high wind profile. (a) Wind speed. (b, c) Frequency of the COI. (d) Active Power of the ESS.

of the controllers is not affected by the change in the operating condition that derives from the disconnection of the load. All three control strategies appear thus robust with respect to the loss of load considered in this study.

Figure 7(d) depicts the active power consumed/provided by the ESS. The SMC shows relatively high oscillations after the disturbance, due to the time that this controller requires to reach the sliding surface. For the H_∞ technique, on the other hand, shows a quicker response but, because of that, also a greater storage of energy in the device is required. This fact is relevant if
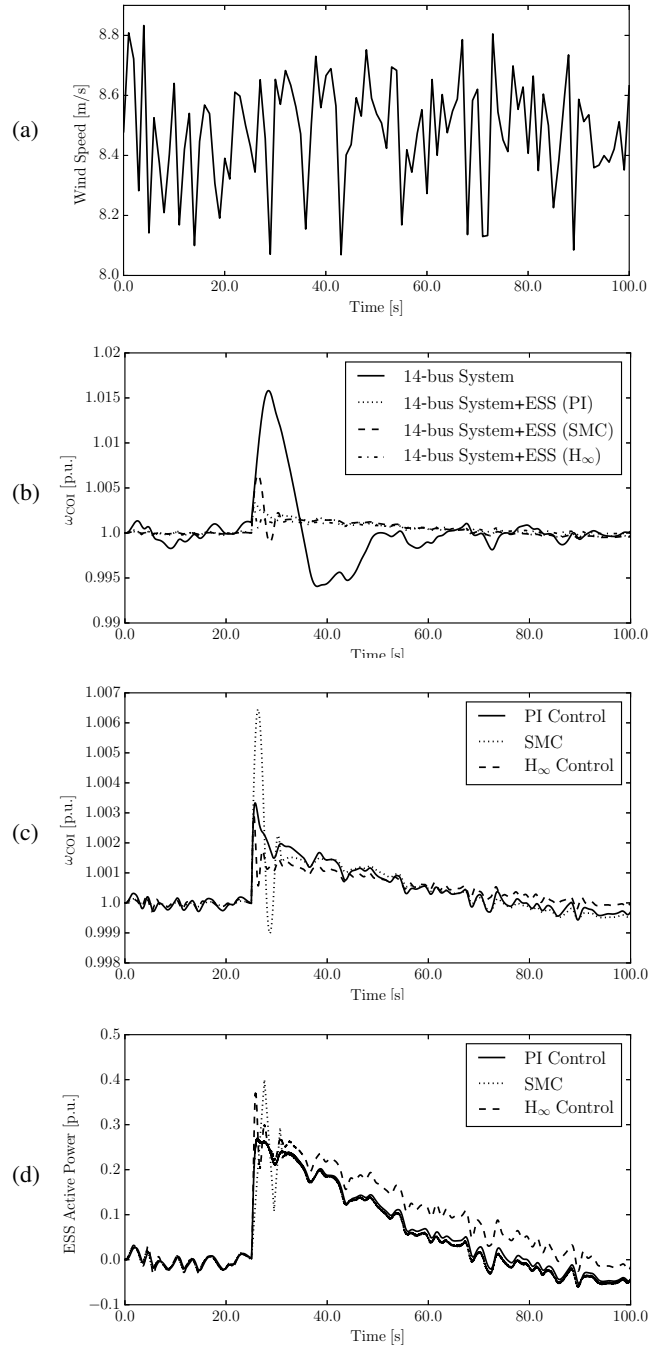
limits of the energy stored in the device are considered. Figure 8 shows the response of the system for the same scenario as in Fig. 7, except for the initial state of charge of the ESS, that is assumed to be closer to its upper limit. At about $t = 60$ s, the storage device regulated by the H_∞ control is not able to store more energy, causing a variation in the frequency of greater amplitude than after the loss of the load.
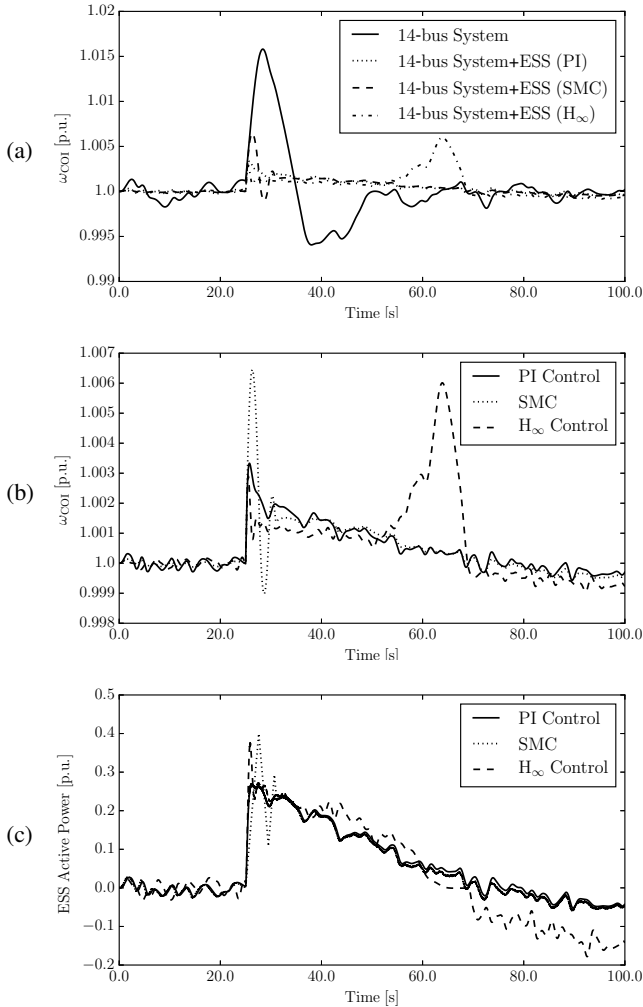
Figure 8: Response of the 14-bus system with an ESS following the loss of the load at bus 9 for a high wind profile and considering energy limits of the storage device. (a), (b) Frequency of the COI. (c) Active Power of the ESS.

V. CONCLUSIONS

In this paper, different control strategies for energy storage devices are discussed and compared. In particular, this paper focuses on the commonly-used PI control, as well as on the more advanced and robust Sliding Mode and H_∞ controllers. The features of these control strategies are highlighted, and their formulation and implementation are explained in detail. Simulation results based on the IEEE 14-bus test system show the overall good performance of each technique, including the PI-based control, when perturbations and contingencies of different nature affects the system. H_∞ controller proves to regulate slightly better than the others, but is more sensitive to energy saturations of the storage device.

Future work will be devoted to improve the comparison presented in this apper. The performance of the control techniques considering a statistical analysis, e.g., hundreds of scenarios, on a real-world system, e.g., the Irish System will be examined in depth. The impact of different control strategies on different ESS technologies, i.e., characterized by different dynamic responses, will be also considered.

REFERENCES

[1] M. G. Molina, P. E. Mercado, and E. H. Watanabe, "Improved Superconducting Magnetic Energy Storage (SMES) Controller for High-Power Utility Applications," *IEEE Transactions on Energy Conversion*, vol. 26, no. 2, pp. 444 – 456, Jun. 2011.

[2] G. Li, S. Cheng, J. Wen, Y. Pan, and J. Ma, "Power System Stability Enhancement by a Double-fed Induction Machine with a Flywheel Energy Storage System," in *Power Engineering Society General Meeting, IEEE*, Montreal, Que, 2006.

[3] F. A. Inthamoussou, J. Pegueroles-Queralt, and F. D. Bianchi, "Control of a Supercapacitor Energy Storage System for Microgrid Applications," *IEEE Transactions on Energy Conversion*, vol. 28, no. 3, pp. 690–697, Sep. 2013.

[4] D. Kairous and R. Wamkeue, "DFIG-based fuzzy sliding-mode control of WECS with a flywheel energy storage," *Electric Power System Research*, vol. 93, pp. 16–23, Dec. 2012.

[5] A. Etxeberria, I. Vechiu, H. Camblong, and J.-M. Vinassa, "Comparison of Sliding Mode and PI Control of a Hybrid Energy Storage System in a Microgrid Application," in *International Conference on Smart Grid and Clean Energy Technologies*, Chengdu, China, Sep. 2011, pp. 966–974.

[6] V. P. Singh, S. R. Mohanty, N. Kishor, and P. K. Ray, "Robust H-infinity load frequency control in hybrid distributed generation system," *Electrical Power & Energy Systems*, vol. 46, pp. 294–305, 2013.

[7] D. Zhu and G. Hug-Glanzmann, "Robust Control Design for Integration of Energy Storage into Frequency Regulation," in *Innovative Smart Grid Technologies (ISGT Europe), 3rd IEEE PES International Conference and Exhibition*, Berlin, Oct. 2012, pp. 1–8.

[8] T. D. Nguyen, K. J. Tseng, C. Zhang, S. Zhang, and H. T. Nguyen, "Model predictive control of a novel axial flux permanent magnet machine for flywheel energy storage system," in *IPEC, 2010 Conference Proceedings*, Oct 2010, pp. 519–524.

[9] C. Trabert, A. Ulbig, and G. Andersson, "Model predictive frequency control employing stability constraints," in *American Control Conference (ACC), 2015*, July 2015, pp. 5678–5685.

[10] K. Zhang, C. Mao, J. Lu, D. Wang, X. Chen, and J. Zhang, "Optimal control of state-of-charge of superconducting magnetic energy storage for wind power system," vol. 8, no. 1, pp. 58–66, Jan. 2014.

[11] Á. Ortega and F. Milano, "Generalized Model of VSC-based Energy Storage Systems for Transient Stability Analysis," *IEEE Transactions on Power Systems*, 2015, (in press). [Online]. Available: arXiv:1509.05290

[12] A. Yazdani and R. Iravani, *Voltage-Sourced Converters in Power Systems. Modeling, Control and Applications*, 1st ed. Wiley-IEEE Press, 2010.

[13] D. N. Kosterev, "Modeling Synchronous Voltage Source Converters in Transmission System Planning Studies," *IEEE Transactions on Power Delivery*, vol. 12, no. 2, pp. 947–952, Apr. 1997.

[14] E. Uzunovic, C. A. Cañizares and J. Reeve, "Fundamental Frequency Model of Static Synchronous Compensator," in *29th North American Power Symposium (NAPS)*, Laramie, Wyoming, Oct. 1997, pp. 49–54.

[15] E. Acha and B. Kazemtabrizi, "A New STATCOM Model for Power Flows Using the NewtonRaphson Method," *IEEE Transactions on Power Systems*, vol. 28, no. 3, pp. 2455–2465, Aug. 2013.

[16] P. Aristidou, D. Fabozzi, and T. V. Cutsem, "Dynamic Simulation of Large-Scale Power Systems Using a Parallel Schur-Complement-Based Decomposition Method," *IEEE Transactions on Parallel and Distributed Systems*, vol. 25, no. 10, pp. 2561–2570, Oct. 2014.

[17] Á. Ortega and F. Milano, "Design of a Control Limiter to Improve the Dynamic Response of Energy Storage Systems," in *Power Engineering Society General Meeting, IEEE*, Denver, Colorado, USA, July 2015.

[18] V. Utkin, J. Guldner, and J. Shi, *Sliding Mode Control in Electro-Mechanical Systems*, 2nd ed. CRC Press, 2009.

[19] S. P. Bhattacharyya, H. Chapellat, and L. H. Keel, *Robust Control: The Parametric Approach*. Prentice Hall, Jun. 1995, ch. 13.

[20] P. Benner, V. Mehrmann, V. Sima, S. Van Huffel, and A. Varga, "SLICOT – A Subroutine Library in Systems and Control Theory," *Applied and Computational Control, Signal and Circuits*, vol. 1, no. 10, pp. 499–539, Nov. 1999.

[21] S. K. M. Kodsi and C. A. Cañizares, "Modeling and Simulation of IEEE 14-bus System with FACTS Controllers," University of Waterloo, Waterloo, Tech. Rep. 2003-3, Mar. 2003.

[22] F. Milano, *Power System Modelling and Scripting*. London: Springer, 2010.

[23] A. Chauhan and R. Saini, "Statistical Analysis of Wind Speed Data Using Weibull Distribution Parameters," in *1st International Conference on Non Conventional Energy (ICONCE 2014)*, Kalyani, India, Jan. 2014, pp. 160–163.